International Journal of Nanomedicine

Dovepress
open access to scientific and medical research

Open Access Full Text Article

ORIGINAL RESEARCH

Effect of nanostructured TiO_2 crystal phase on photoinduced apoptosis of breast cancer epithelial cells

This article was published in the following Dove Press journal:
International Journal of Nanomedicine
3 July 2014
Number of times this article has been viewed

Nefeli Lagopati[1,2]
Effie-Photini Tsilibary[1,*]
Polycarpos Falaras[2,*]
Panagiota Papazafiri[3]
Evangelia A Pavlatou[4]
Eleni Kotsopoulou[1]
Paraskevi Kitsiou[1,*]

[1]Institute of Biosciences and Applications, [2]Institute of Advanced Materials, Physicochemical Processes, Nanotechnology and Microsystems, National Center for Scientific Research "Demokritos", Athens, Greece; [3]Department of Animal and Human Physiology, Faculty of Biology, School of Science, National and Kapodistrian University of Athens, Athens, Greece; [4]Laboratory of General Chemistry, School of Chemical Engineering, National Technical University of Athens, Athens, Greece

*These authors contributed equally to this work

Purpose: The use of nanoparticles has seen exponential growth in the area of health care, due to the unique physicochemical properties of nanomaterials that make them desirable for medical applications. The aim of this study was to examine the effects of crystal phase-nanostructured titanium dioxide particles on bioactivity/cytotoxicity in breast cancer epithelial cells.

Materials and methods: Cultured Michigan Cancer Foundation (MCF)-7 and human breast adenocarcinoma (MDA-MB-468) breast cancer epithelial cells were exposed to ultraviolet A light (wavelength 350 nm) for 20 minutes in the presence of aqueous dispersions of two different nanostructured titanium dioxide (TiO_2) crystal phases: anatase and an anatase–rutile mixture. Detailed characterization of each titanium dispersion was performed by dynamic light scattering. A 3-(4,5-dimethylthiazol-2-yl)-2,5 diphenyltetrazolium bromide (MTT) colorimetric assay was employed to estimate the percentage of viable cells after each treatment. Western blot analysis of protein expression and characterization, as well as a deoxyribonucleic acid (DNA)-laddering assay, were used to detect cell apoptosis.

Results: Our results documented that 100% anatase TiO_2 nanoparticles (110–130 nm) exhibited significantly higher cytotoxicity in the highly malignant MDA-MB-468 cancer cells than anatase–rutile mixtures (75%/25%) with the same size. On the contrary, MCF-7 cells (characterized by low invasive properties) were not considerably affected. Exposure of MDA-MB-468 cells to pure anatase nanoparticles or anatase–rutile mixtures for 48 hours resulted in increased proapoptotic Bax expression, caspase-mediated poly(adenosine diphosphate ribose) polymerase (PARP) cleavage, DNA fragmentation, and programmed cell death/apoptosis.

Conclusion: The obtained results indicated that pure anatase TiO_2 nanoparticles exhibit superior cytotoxic effects compared to anatase–rutile mixtures of the same size. The molecular mechanism of TiO_2 nanoparticle cytotoxicity involved increased Bax expression and caspase-mediated PARP inactivation, thus resulting in DNA fragmentation and cell apoptosis.

Keywords: nanostructured TiO_2, anatase, rutile, photocatalysis, breast cancer epithelial cells, apoptosis

Introduction

Nanoparticles have unique physicochemical properties and functionalities that are different from their bulk counterparts.[1,2] In recent years, there has been increased concern about nanotoxicology and the factors that are intertwined with it. Due to the importance of this size class of particles, there is a need for clarification and better understanding of nanoparticle physicochemical properties and their cytotoxic potential.[3–5]

Titanium is widely used in biomedical applications, due to its mechanical properties and biocompatibility, and of course for photocatalysis purposes.[6,7] It is now well established that photoexcited titanium dioxide (TiO_2) can drive various chemical

Correspondence: Paraskevi Kitsiou
Institute of Biosciences and Applications, National Center for Scientific Research "Demokritos", corner Patriarchou Grigoriou and Neapoleos Streets, Aghia Paraskevi, Attiki, Athens 15310, Greece
Tel +30 21 0650 3615
Fax +30 21 0651 1767
Email pkit@bio.demokritos.gr

reactions due to its strong oxidizing and reducing ability and can also affect cellular functions,[8,9] thus allowing applications in cancer cell treatment[10] and sterilization of various surfaces.[11]

Recent studies have demonstrated that TiO_2 induces death by apoptosis in different types of cells, such as mesenchymal stem cells,[12] osteoblasts,[13] and other cell types. Furthermore, the photocatalytic properties of TiO_2-mediated toxicity have been shown to eradicate several types of cancer cells[8,14,15] upon irradiation with light of wavelength <390 nm via the mechanism of oxidative stress. Photon energy generates pairs of electrons and holes that react with water and oxygen into the cells to yield reactive oxygen species (ROS), which have been proved to damage preferentially cancer cells.[16–18] Consequently, we investigated the possibility for use of TiO_2 as an anticancer agent in the presence of ultraviolet (UV)-A light.

There is still uncertainty in the current understanding of the relationship between physicochemical parameters and potential toxicological effects. There have been several recent studies on the toxicity evaluation of nanosized TiO_2, establishing a relationship between toxicity and physicochemical characteristics.[3,4,9,19,20] For example, Warheit et al recently exposed the lungs of rats to three different sizes of TiO_2 nanoparticles, and reported that toxicity does not depend on particle size or surface area.[19] On the contrary, Oberdörster et al[3–5] conducted pulmonary toxicity tests with 20 nm (80% anatase) and 250 nm (100% anatase) TiO_2 particles, and observed that total surface area was a parameter related to neutrophil-mediated lung inflammation in rats. In addition, Jiang et al[21] demonstrated that 100% anatase TiO_2 particles induced higher ROS activities compared to anatase–rutile mixtures of the same size. Furthermore, toxicological effects are usually evaluated by in vitro and in vivo studies to determine the intrinsic potential of particles to generate ROS.[22] Both in vitro and in vivo tests of engineered nanoparticles (eg, carbon nanotubes, TiO_2, and quantum dots) indicate that their toxicity is related to ROS production.[23,24] Therefore, no clear trends regarding the influence of TiO_2 crystallinity and particle size on biological activity could be seen in these different studies, whereas conflicting results were reported.

Based on the hypothesis that crystallinity will impact oxidant generation, the aim of this study was to examine the effect of the particle crystal phase of a model nanoparticle, TiO_2, on the cytotoxic activity of TiO_2 dispersions; these contained nanoparticles of similar sizes and different nanostructured crystal phases: anatase (100%) and an anatase–rutile mixture (75%/25%). The cytotoxic effects of nanoparticles were examined using two cancer cell lines: MDA-MB-468 (human breast adenocarcinoma, highly invasive) and Michigan Cancer Foundation (MCF)-7 (low metastatic potential), both derived from breast epithelium. We also investigated the underlying mechanisms of cytotoxicity induced by TiO_2-nanoparticle dispersions.

Materials and methods

Cell culture

Human breast epithelial cells (MCF-7 and MDA-MB-468) were cultured in 75 cm^2 flasks in Dulbecco's Modified Eagle's Medium supplemented with 10% fetal bovine serum, 1% L-glutamine, 1% sodium pyruvate, and antibiotics (all media were purchased from Merck KGaA, Darmstadt, Germany), and incubated at 37°C in a 5% CO_2 incubator. Also, trypsin–ethylenediaminetetraacetic acid (EDTA) 0.05%:0.02% (weight/volume) (Thermo Fisher Scientific, Waltham, MA, USA) was used for trypsinization of cells.

Preparation of TiO_2 dispersions

For the preparation of TiO_2 P25 (anatase 75%–rutile 25% mixture, specific surface area 55 m^2/g; Evonik Industries, Essen, Germany) and TiO_2 (100% anatase, specific surface area 200–220 m^2/g; Sigma-Aldrich Co., St Louis, MO, USA) dispersions, nanoparticles were added to double-distilled water, in order to form a dispersion of final concentration of about 100 μM. Then, they were rigorously stirred for 30 minutes.

Characterization of TiO_2 dispersions

For the characterization of Evonik TiO_2 P25 and Sigma-Aldrich TiO_2 100% anatase nanoparticles, 20 μM dispersions were prepared and stirred for 30 minutes. Fragmentation of aggregates, formed between nanoparticles, was then achieved by using ultrasound of maximum tension for about an hour.

Dynamic light scattering (DLS; also known as photon-correlation spectroscopy or quasielastic light scattering) was used to determine the size-distribution profile of small particles in suspension or solution,[25] as well as other physicochemical properties, such as zeta potential. The fundamentals of this method are based on the fact that when light hits small particles, it scatters in all directions (Rayleigh scattering), as long as the particles are small compared to the wavelength (below 250 nm). In the case of laser as a light source, which

is monochromatic and coherent, a time-dependent fluctuation in scattering intensity is observed.

In particular, DLS measurements were performed on aged titanium dispersions (10 days after preparation) after filtering the solutions through a 0.45 μm filter (Merck Millipore), in order to estimate size at 25°C, with a rate of approximately 170 kilocounts/second, attenuator at the seventh level, and measurement duration of 80 seconds. Sample preparation, either by filtration or centrifugation, was performed in order to remove dust and artifacts from the solution.

Also, measurements for zeta potential were performed, at 25°C, with a rate of approximately 300 kilocounts/second, attenuator at the seventh level, and 12 zeta runs. An ALV/CGS-3 compact goniometer system (ALV, Hesse, Germany) was used, equipped with an He–Ne laser, operating at 632.8 nm, which was interfaced with an ALV-5000/EPP multi-tau digital correlator with 288 channels and an ALV/LSE-5003 light-scattering electronics unit for stepper-motor drive and limit-switch control.

Cell-viability analysis (MTT assay)

The 3-(4,5-dimethylthiazol-2-yl)-2,5-diphenyl-tetrazolium bromide (MTT) colorimetric assay was used to determine cell viability. The MTT assay[26] is based on the ability of a mitochondrial dehydrogenase enzyme from viable cells to cleave the tetrazolium rings of the pale-yellow MTT and form dark-blue formazan crystals that are largely impermeable to cell membranes, thus resulting in crystal accumulation within healthy cells. Lysis of cells by the addition of a detergent results in the liberation of the crystals, which then become soluble. The number of viable cells is directly proportional to the level of the formazan product created. The color was quantified using a simple colorimetric assay, with the use of a multiwell scanning spectrophotometer (enzyme-linked immunosorbent assay reader).[27]

For the MTT assays, MCF-7 and MDA-MB-468 cancer breast cells (~6,000 cells/well) were seeded in 96-well plates, using Dulbecco's Modified Eagle's Medium, as previously mentioned. Twenty-four hours after plating, various concentrations of the two TiO_2 dispersions of different crystal structure were added to the appropriate samples, and the samples were irradiated using UVA light (wavelength 350 nm) for 20 minutes. The cells were further cultured for 48 hours. On the day of the viability assay, fresh medium (~100 μL/well) and MTT solution (5 mg/mL in phosphate-buffered-saline [PBS]) was added to each well, and the plates were incubated at 37°C for at least 3 hours. At the end of the incubation period, the medium and MTT solution were removed from each well and dimethyl sulfoxide was added. The 96-well plates were then gently shaken for 30 minutes. In this type of experiment, optical density was measured at 590 nm. The percentage of viability was calculated compared with untreated control (100% viability).

The experiment was repeated several times, in order to determine the minimal time of UV activation of titanium dispersions and the optimal concentration of TiO_2. The appropriate conditions were selected, and the experiment for examining titanium effects repeated at least five times in quadruplicate. In all instances, similar results were obtained.

Western blotting

To examine the effects of TiO_2 dispersions on caspase-mediated poly(adenosine diphosphate ribose) polymerase (PARP) cleavage indicating selective cell apoptosis, Western blotting experiments were performed. Cells were scraped into PBS, washed twice with PBS, resuspended in 3-([3-cholamidopropyl]dimethylammonio)-1-propanesulfonate buffer containing a 1% (volume/volume) protease-inhibitor cocktail (P8340; Sigma-Aldrich) and lysed by repeated (three times) freezing and thawing.

The expression of Bcl-2, Bax, Bad, and Bcl-x_L and assessment of their levels was also studied. Cells were washed in PBS and lysed in lysis buffer containing 20 mM Tris-HCl (pH 7.5), 1% Triton X-100, 150 mM NaCl, 1 mM EDTA (pH 8.0), 10 mM NaF, 1 mM Na_2VO_4, 1 mM PMSF (phenyl methyl sulfonyl fluoride), and the protease-inhibitor cocktail.

A Bradford colorimetric assay (Thermo Fisher Scientific) was utilized to estimate total protein concentration. Equal amounts of total protein of cell lysates were separated by sodium dodecyl sulfate (SDS) polyacrylamide gel electrophoresis and transferred to Hybond enhanced chemiluminescence nitrocellulose membranes (GE Healthcare UK Ltd, Little Chalfont, UK). Membranes were probed with anti-PARP (9542; Cell Signaling Technology, Danvers, MA, USA), anti-Bcl-2 (sc-7382), anti-Bcl-x_L (sc-8392), anti-Bax (sc-6236), and anti-Bad (sc-942) (Santa Cruz Biotechnology, Dallas, TX, USA) antibodies. Proteins were detected with an enhanced chemiluminescence detection system (Thermo Fisher Scientific) after incubation with horseradish peroxidase-conjugated secondary antibodies (GE Healthcare). To ensure equal amounts of protein loading, the blots were stripped (Re-Blot Plus Western blot stripping solution; Merck Millipore) and reprobed with anti-β-tubulin monoclonal antibodies.

Results were obtained from three independent experiments for each type of TiO_2 dispersion.

DNA-laddering assay

To establish the effects of TiO_2 dispersions on apoptotic cell death, deoxyribonucleic acid (DNA) was isolated, electrophoresed in agarose gel, and images of intact and/or laddered DNA were obtained. Briefly, cells were gently scraped in culture medium and centrifuged at approximately 2,000 rpm at room temperature. The pellet was then washed in PBS, centrifuged again, and cells lysed in DNA-extraction buffer containing 1% nonyl phenoxypolyethoxylethanol (NP)-40, 1% SDS, 10 mM EDTA, and 50 mM Tris-HCl (pH 7.5). Subsequently, ribonuclease A and proteinase K were added and the lysates left overnight at 50°C. Ammonium acetate (2.5 M) was then added and lysates mixed thoroughly. DNA was precipitated with ice-cold ethanol, and the pellet was washed again in ethanol, air-dried at room temperature, and dissolved in Tris–EDTA buffer containing 1 mM EDTA and 10 mM Tris-HCl (pH 7.4). DNA concentration was determined, and samples were loaded in 1.5%–2% agarose gel stained with 0.5 µg/mL ethidium bromide. Agarose gels were run at 100 V for the appropriate time. DNA patterns were visualized by UV-illumination.

Statistical analysis

Values are presented as means ± standard deviation. Statistically significant differences between values were evaluated by one-way analysis of variance and the nonparametric Kruskal–Wallis method in the SPSS program (IBM Corporation, Armonk, NY, USA) as appropriate. $P<0.05$ was considered statistically significant.

Results

Photocatalyst characterization

DLS provides insight into the dynamic properties of soft materials by measuring single scattering events, meaning that each detected photon has been scattered by the sample exactly once. Actually, DLS makes use of spectral analysis in order to observe the dynamic properties that characterize colloidal dispersions of particles, and it is a commonly used technique for the determination of particle size in the submicron range. In this study, DLS was used to characterize the size and zeta potential of Evonik TiO_2 P25 and Sigma-Aldrich TiO_2 (100% anatase) nanoparticles.

The pH of Sigma-Aldrich TiO_2 (100% anatase) was 6.8, and the pH of Evonik TiO_2 P25 was 7.1. The distribution of their size as a function of intensity is shown in Figure 1, A and C, and the zeta potential in Figure 1, B and D, respectively. The same mean values were estimated by DLS analysis of size, as a function of volume, and as a function of number of nanoparticles (data not shown).

The average size was about 111.3 nm for TiO_2 100% anatase and 138.5 nm for Evonik TiO_2 P25 (Figure 1, A and C). Figure 1B shows that there are four distinct peaks dividing the zeta potential (peak 1, –33.1 mV; peak 2, –20.8 mV; peak 3, –10.9 mV; peak 4, –2 mV) of TiO_2 100% anatase, with zeta potential of –16.7±9 mV, while in the case of Evonik

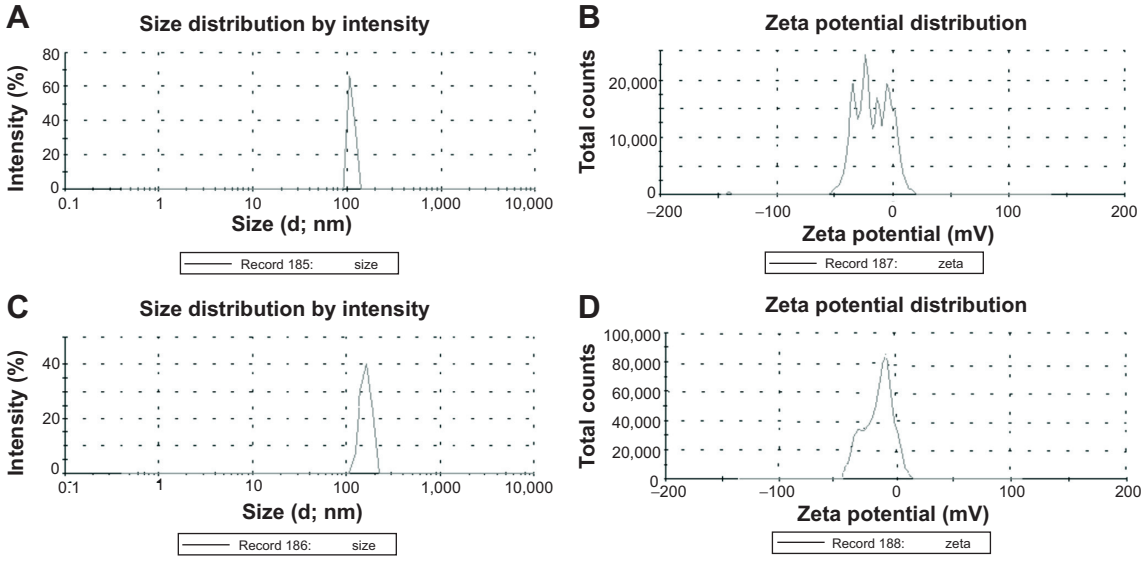

Figure 1 Characterization of TiO_2 nanoparticles.
Notes: Distribution of the hydrodynamic diameter (d, or $2R_h$) of (**A**) Sigma-Aldrich TiO_2 100% anatase and (**C**) Evonik TiO_2 P25 nanoparticles obtained by DLS. Distribution of zeta potential of (**B**) Sigma-Aldrich TiO_2 100% anatase and (**D**) Evonik TiO_2 P25 nanoparticles obtained by DLS. Analysis was performed from the stock solution. Evonik TiO_2 P25; Evonik Industries, Essen, Germany. Sigma-Aldrich TiO_2; Sigma-Aldrich Co., St Louis, MO, USA.
Abbreviation: DLS, dynamic light scattering.

TiO_2 P25 there are two peaks (peak 1, –23.7 mV; peak 2, –9.09 mV) with zeta potential of –11.7±8 mV (Figure 1D).

Additionally, micro-Raman spectra were recorded in the backscattering configuration using an inVia Reflex system (Renishaw, Wotton-under-Edge, UK) equipped with a diode laser at 785 nm excitation (Figure 2). The scattered light was filtered by a dielectric edge Rayleigh rejection filter with cutoff at 100 cm^{-1} and analyzed with a 1,200 line/mm diffraction grating. The laser beam was focused on the sample surface using the long working distance (8 mm) objective with magnification of 50× with a DM LM microscope (Leica Microsystems, Wetzlar, Germany). The nominal spot size of the laser beam was about 1 µm, and the power density on the sample was controlled to 0.5 mW/μm^2 with a filter.

The spectra of the Sigma-Aldrich TiO_2 show only the anatase-vibration peaks centered at 144, 196, 394, 516 and 637 cm^{-1}. Besides anatase, the Raman spectra of Evonik P25 also show the presence of the rutile TiO_2 phase, evidenced by two extra broad peaks at 446 and 612 cm^{-1}. Neither position (144 cm^{-1}) nor line width (9.5 cm^{-1}) of the strongest anatase Raman mode showed any difference for the two samples, and were characteristic for large crystal size, above 20 nm (Figure 2).

Effect of photoexcited TiO_2 nanoparticles on cell viability

The MTT assay was utilized to evaluate the effects of TiO_2 on the viability of both MCF-7 and MDA-MB-468 cells. Cells were incubated with increasing concentrations of

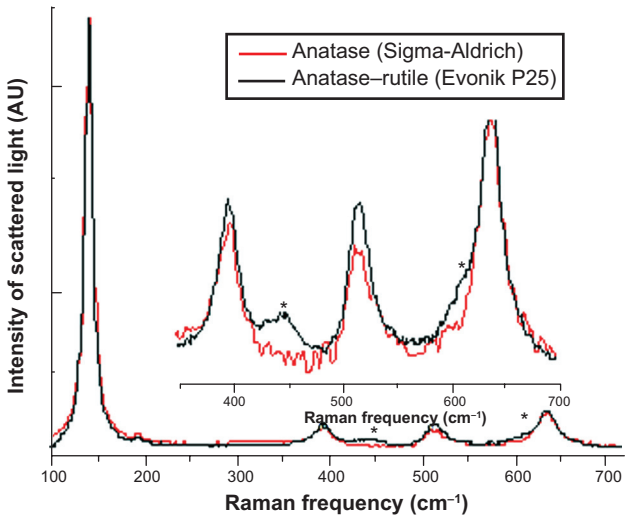

Figure 2 Raman spectra of TiO_2 100% anatase and Evonik TiO_2 P25 nanoparticles.
Notes: The inset shows a magnified view of 350–700 cm^{-1} of the Raman spectra. *The area of Raman spectra where the rutile TiO_2 phase became evident. Analysis was performed from the stock solution. Evonik TiO_2 P25; Evonik Industries, Essen, Germany. Sigma-Aldrich TiO_2; Sigma-Aldrich Co., St Louis, MO, USA.
Abbreviation: AU, arbitary units.

TiO_2 dispersions (100% anatase or anatase 75%–rutile 25% mixture) for 48 hours, and the percentage of cell viability was estimated as a function of the photocatalyst concentration. Cell viability (L) was calculated as $L \pm \delta L$ by the following equations:

$$L = \frac{ABS_{treated}}{ABS_{untreated}} \times 100\% \quad (1)$$

and

$$\delta L = \sqrt{\left(\frac{\partial L}{\partial ABS_{treated}}\delta ABS_{treated}\right)^2 + \left(\frac{\partial L}{\partial ABS_{untreated}}\delta ABS_{untreated}\right)^2} \quad (2)$$

where $ABS_{treated}$ and $ABS_{untreated}$ are the mean absorption values at 590 nm for the treated and untreated samples, respectively.

As shown in Figure 3A, cell viability gradually decreased as the concentration of Sigma-Aldrich TiO_2 100% anatase increased. In particular, a concentration of 20 µM TiO_2 reduced MDA-MB-468 cell viability by 45%, while the same dose affected only 25% of the MCF-7 cell population (Figure 3A). The effect of Sigma-Aldrich TiO_2 100% anatase on cell viability was further enhanced by UV irradiation (Figure 3C). In the presence of 20 µM of UVA-irradiated TiO_2 100% anatase, MDA-MB-468 cell viability was reduced by 70%, while the same dose affected 40% of MCF-7 cells (Figure 3C).

In addition, a progressive reduction in cell viability was observed in the presence of increased doses of Evonik TiO_2 P25. Specifically in the case of MDA-MB-468 cells, a concentration of 20 µM reduced cell viability to 60%, while the relevant percentage of MCF-7 cell viability was 80% (Figure 3B). In the presence of 20 µM of UVA-irradiated Evonik TiO_2 P25, MDA-MB-468 cells exhibited 40% viability, whereas the corresponding percentage in MCF-7 cells was 80% (Figure 3D). UV irradiation by itself exerted a minor effect on cell viability (about 10%) (Figure 3, C and D).

Taken together, these results indicate that the highly malignant MDA-MB-468 cancer cells are more susceptible to cell death when exposed to UVA-activated TiO_2 nanoparticles compared to MCF-7 cells, which are characterized by low metastatic potential. Moreover, TiO_2 composed of 100% anatase had a higher cytotoxic effect compared to the effect of Evonik TiO_2 P25.

Effect of photoexcited TiO_2 nanoparticles on caspase-mediated PARP cleavage

Activation of caspases is associated with morphological and functional changes taking place during cell apoptosis. PARP (113 kDa), is one of the main cleavage targets of activated

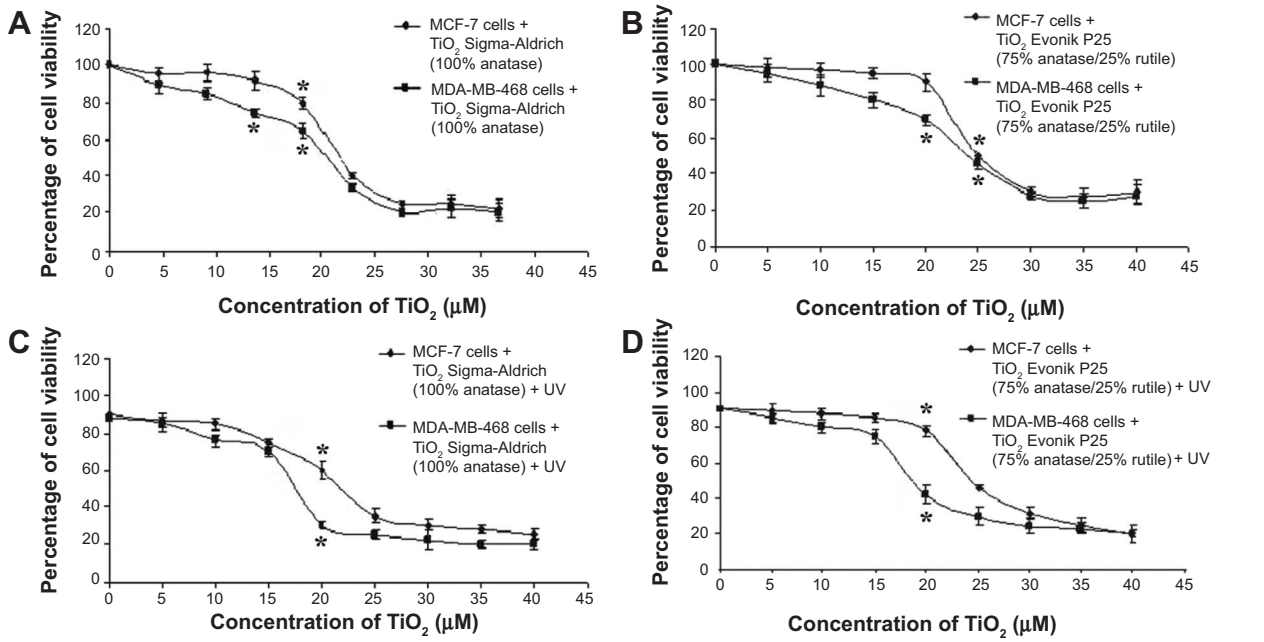

Figure 3 Effect of photoexcited TiO_2 nanoparticles on MCF-7 and MDA-MB-468 breast cancer epithelial cell viability.
Notes: **(A)** Effect of Sigma-Aldrich TiO_2 concentration on cell viability; **(B)** effect of Evonik TiO_2 P25 concentration on cell viability; **(C)** effect of UVA-irradiated Sigma-Aldrich TiO_2 on cell viability; **(D)** effect of UVA-irradiated Evonik TiO_2 P25 on cell viability. *$P<0.05$ compared to control (untreated) cells. Cell viability was determined by the MTT assay. Data represent means ± standard deviation from five independent experiments. Evonik TiO_2 P25; Evonik Industries, Essen, Germany. Sigma-Aldrich TiO_2; Sigma-Aldrich Co., St Louis, MO, USA.
Abbreviations: MCF, Michigan Cancer Foundation; MDA-MB-468, human breast adenocarcinoma; UV, ultraviolet; MTT, 3-(4,5-dimethylthiazol-2-yl)-2,5-diphenyltetrazolium bromide.

caspases, and participates in DNA repair following exposure to stress.[28–30] Cleavage of PARP results in loss of the enzymatic DNA-repair function,[31] thus providing a marker of cells undergoing apoptosis.[32]

PARP cleavage was examined by Western blot analysis in cells treated with UV-activated dispersions of Evonik TiO_2 P25 or Sigma-Aldrich TiO_2 100% anatase. Lysates from cells treated for 24 hours with cisplatin (1 mg/mL) were used as a positive control for the induction of PARP cleavage. As shown in Figure 4, A and B, in cells treated with Sigma-Aldrich TiO_2 100% anatase or photoexcited TiO_2 nanoparticles, PARP cleavage was remarkably increased compared to control cells, confirming that treatment with Sigma-Aldrich TiO_2 100% anatase nanoparticles induced apoptosis in MDA-MB-468 cells; on the contrary, TiO_2 100% anatase did not affect PARP cleavage in MCF-7 cells (Figure 4, C and D). Figure 5, A and B show that only photoexcited Evonik TiO_2 P25 treatment resulted in PARP cleavage in MDA-MB-468 cells compared to the control group. However, the effect of photoexcited Evonik TiO_2 P25 on PARP cleavage was less than that obtained by TiO_2 100% anatase. PARP cleavage was not detected in MCF-7 cells under the same conditions (Figure 5, C and D).

In summary, our results indicated that photoexcited TiO_2 nanoparticles induced apoptosis specifically in MDA-MB-468 cells. This effect was enhanced in cells treated with TiO_2 100% anatase nanoparticles compared to cells treated with Evonik P25 TiO_2.

Effect of photoexcited TiO_2 nanoparticles on Bcl-2 family protein expression

Bcl-2 family proteins play a pivotal role in the regulation of cell apoptosis. It is also argued that some Bcl-2 family proteins can induce (proapoptotic members) or inhibit (antiapoptotic members) the release of cytochrome C into the cytosol, which in turn activates caspase-9 and caspase-3, thus leading to apoptosis.[33,34]

Therefore, we examined the effects of TiO_2 on the expression of Bcl-2, Bcl-x_L (antiapoptotic factors), Bax, and Bad (proapoptotic factors). Cells were treated with UV-activated dispersions of Sigma-Aldrich TiO_2 100% anatase and Evonik TiO_2 P25, and cell lysates were immunoblotted with anti-Bcl-2, anti-Bcl-x_L, anti-Bax, and anti-Bad antibodies. Lysates from cells treated for 24 hours with cisplatin (1 mg/mL) were used as a positive control for apoptosis.

Representative Western blots of Bcl-2, Bax, Bcl-x_L, and Bad expression in MDA-MB-468 cells and MCF-7 cells are shown in Figure 6, A and C, respectively. Photoexcited TiO_2 100% anatase and Evonik P25 nanoparticles induced specifically in MDA-MB-468 cells an increase in Bax expression

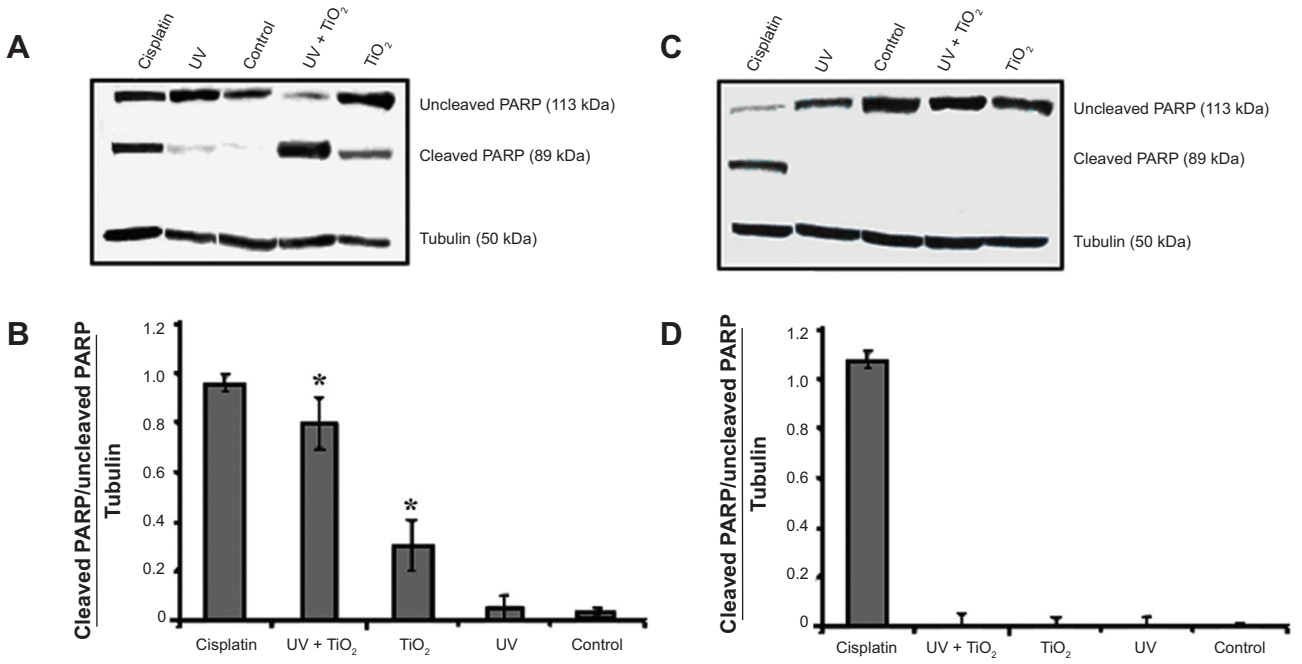

Figure 4 Photoexcited TiO$_2$ 100% anatase (Sigma-Aldrich) nanoparticles induced caspase-mediated PARP cleavage.
Notes: Representative Western blots of uncleaved and cleaved PARP of (**A**) MDA-MB-468 cells and (**C**) MCF-7 cells. Blots were stripped and reprobed with anti-tubulin antibody to normalize the blots for protein levels. Densitometric quantification of cleaved/uncleaved PARP to tubulin levels for (**B**) MDA-MB-468 cells and (**D**) MCF-7 cells. *$P<0.05$ compared to cleaved/uncleaved PARP/tubulin levels of untreated cells. Lysates of cells treated for 24 hours with cisplatin (1 mg/mL) were used as positive control for the induction of PARP cleavage. Data represent means ± standard deviation from three independent experiments. Sigma-Aldrich TiO$_2$; Sigma-Aldrich Co., St Louis, MO, USA.
Abbreviations: MCF, Michigan Cancer Foundation; MDA-MB-468, human breast adenocarcinoma; UV, ultraviolet; PARP, poly(adenosine diphosphate ribose) polymerase.

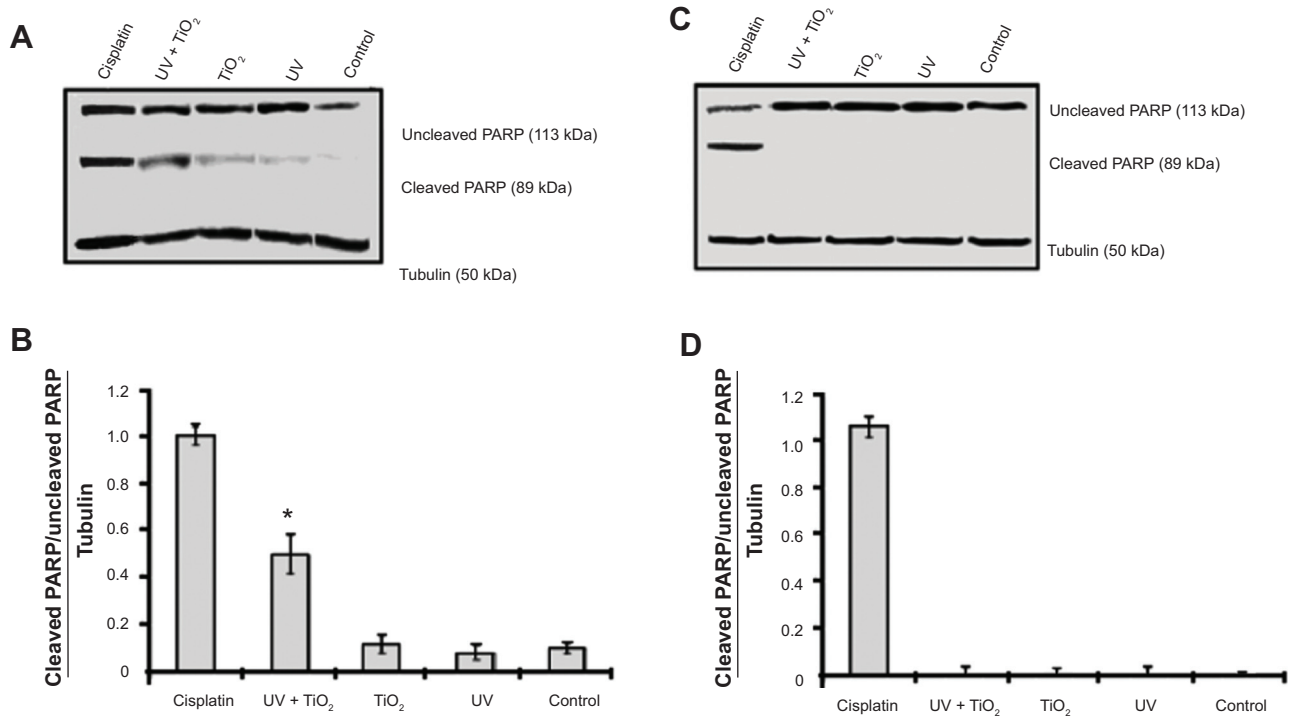

Figure 5 Photoexcited Evonik TiO$_2$ P25 nanoparticles induced caspase-mediated PARP cleavage.
Notes: Representative Western blots of uncleaved and cleaved PARP of (**A**) MDA-MB-468 cells and (**C**) MCF-7 cells. Blots were stripped and reprobed with anti-tubulin antibody to normalize the blots for protein levels. Densitometric quantification of cleaved/uncleaved PARP to tubulin levels for (**B**) MDA-MB-468 cells and (**D**) MCF-7 cells. *$P<0.05$ compared to cleaved/uncleaved PARP/tubulin levels of untreated cells. Lysates of cells treated for 24 hours with cisplatin (1 mg/mL) were used as positive control for the induction of PARP cleavage. Data represent means ± standard deviation from three independent experiments. Evonik TiO$_2$ P25; Evonik Industries, Essen, Germany.
Abbreviations: MCF, Michigan Cancer Foundation; MDA-MB-468, human breast adenocarcinoma; UV, ultraviolet; PARP, poly(adenosine diphosphate ribose) polymerase.

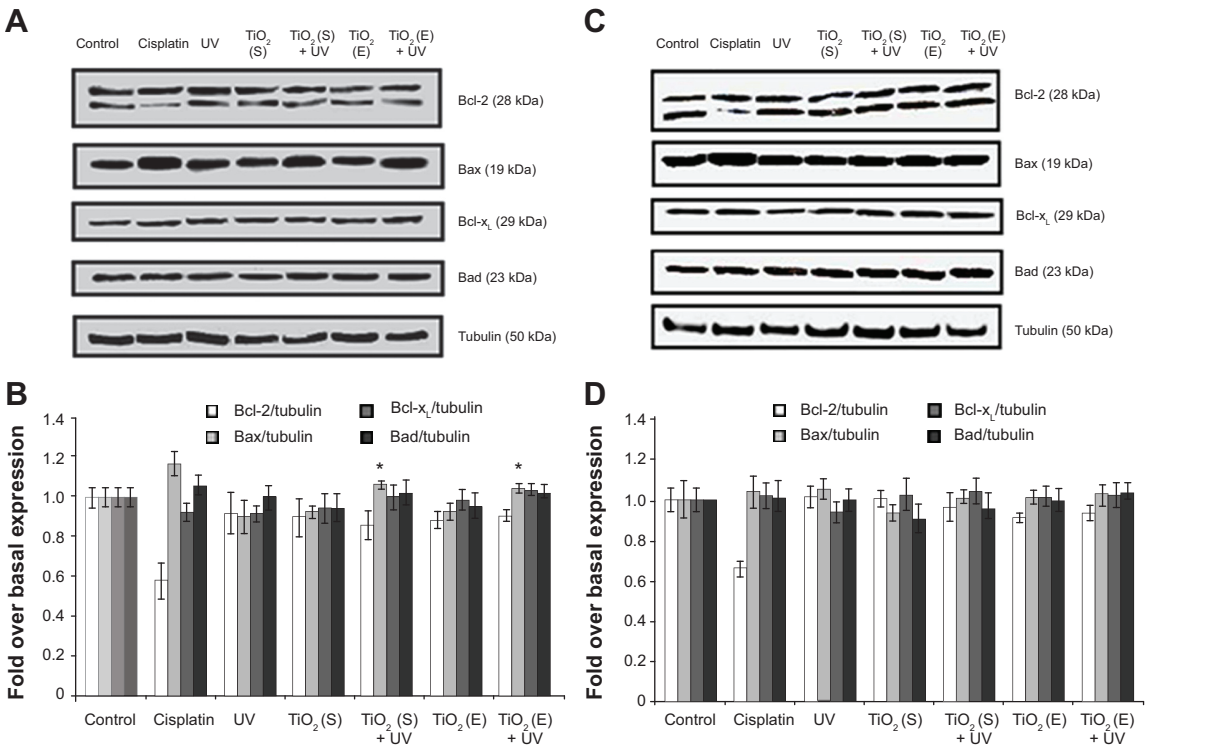

Figure 6 Photoexcited TiO_2 100% anatase and Evonik P25 nanoparticles increased Bax expression in MDA-MB-468 cells.

Notes: Representative Western blots of Bcl-2, Bax, Bcl-x_L, and Bad expression in (**A**) MDA-MB-468 cells and (**C**) MCF-7 cells. Blots were stripped and reprobed with anti-tubulin antibody to normalize the blots for protein levels. Densitometric quantification of Bcl-2/tubulin, Bax/tubulin, Bcl-x_L/tubulin and Bad/tubulin as fold over basal rate (control cells) in (**B**) MDA-MB-468 cells and (**D**) MCF-7 cells. *$P<0.05$ versus control cells. Lysates of cells treated for 24 hours with cisplatin (1 mg/mL) were used as positive control for induction of Bcl-2 family protein expression. Data represent means ± standard deviation from three independent experiments. Evonik TiO_2 P25; Evonik Industries, Essen, Germany. Sigma-Aldrich TiO_2; Sigma-Aldrich Co., St Louis, MO, USA.

Abbreviations: MCF, Michigan Cancer Foundation; MDA-MB-468, human breast adenocarcinoma; UV, ultraviolet; TiO_2 (S), Sigma-Aldrich TiO_2 100% anatase; TiO_2 (E), Evonik TiO_2 P25.

compared with the control group (Figure 6, A and B). Upregulation of Bax expression (apoptosis index) was in agreement with the observed increase in PARP cleavage (Figure 4, A and B and Figure 5, A and B) in these cells. Bcl-2, Bcl-x_L, and Bad expression were not significantly affected by photoexcited TiO_2 nanoparticles (Figure 6, A and B). Treatment of MCF-7 cells with each of the dispersions of photoexcited TiO_2 nanoparticles had no significant effect on the expression of Bcl-2, Bax, Bcl-x_L, or Bad proteins (Figure 6, C and D).

Effect of photoexcited TiO_2 nanoparticles on DNA fragmentation

DNA fragmentation detected by electrophoresis (DNA-laddering assay) is a commonly used method for separation of DNA fragments based on their size and charge.[35–40] Therefore, the effect of TiO_2 nanoparticles on DNA damage in breast cancer epithelial cells was qualitatively evaluated using the DNA-laddering assay. We observed that significant DNA damage (fragmentation) was induced after treatment of MDA-MB-468 cells with photoexcited Sigma-Aldrich TiO_2 100% anatase, although Evonik TiO_2 P25 also induced DNA laddering, but to a lesser extent compared to TiO_2 100% anatase (Figure 7A). The pattern of DNA laddering was similar to that obtained from cells treated for 24 hours with cisplatin (1 mg/mL) (Figure 7A). Control cells or cells treated with either UVA or unirradiated TiO_2 100% anatase exhibited no significant DNA fragmentation, as indicated by the presence of a wide genomic DNA band on the top of agarose gel. In MCF-7 cells, neither Sigma-Aldrich TiO_2 100% anatase nor Evonik TiO_2 P25 induced DNA damage, as indicated by the absence of a DNA-laddering pattern (Figure 7B). Taken together, these results (Figure 7) are well correlated with results obtained from the analysis of PARP cleavage (Figures 4 and 5) and Bax expression (Figure 6) insofar as apoptosis is concerned.

Discussion

The present study demonstrates that the cytotoxicity of TiO_2 nanoparticles depends on the crystal phase of TiO_2 particles, and also establishes the apoptotic potential of TiO_2 nanoparticles in two different breast cancer epithelial cell lines: the highly malignant MDA-MB-468 and MCF-7 cells, which have low metastatic potential.

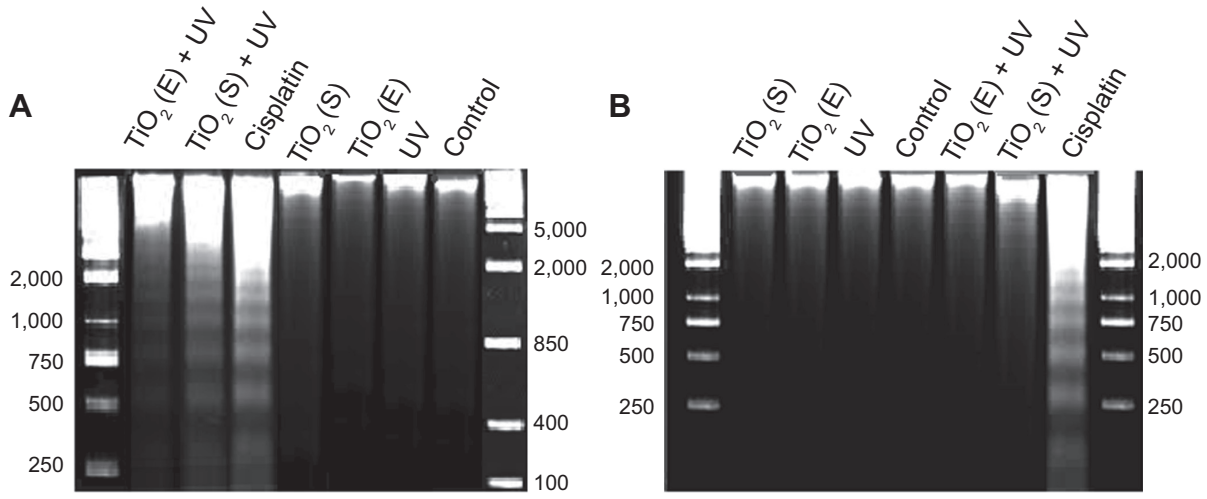

Figure 7 Photoexcited TiO_2 100% anatase and Evonik P25 nanoparticles induced DNA fragmentation (laddering) in MDA-MB-468 cells.
Notes: Representative images of DNA laddering in **(A)** MDA-MB-468 and **(B)** MCF-7 cells, showing the number of base pairs. Cells treated for 24 hours with cisplatin (1 mg/mL) were used as positive control for induction of DNA fragmentation. Evonik TiO_2 P25; Evonik Industries, Essen, Germany. Sigma-Aldrich TiO_2; Sigma-Aldrich Co., St Louis, MO, USA.
Abbreviations: MCF, Michigan Cancer Foundation; MDA-MB-468, human breast adenocarcinoma; UV, ultraviolet; DNA, deoxyribonucleic acid; TiO_2 (S), Sigma-Aldrich TiO_2 100% anatase; TiO_2 (E), Evonik TiO_2 P25.

Previous studies in various animal and human cell lines demonstrated that TiO_2 nanoparticles generate a large amount of hydroxyl free radicals, thereby leading to DNA damage.[41,42] It has been proposed that the genotoxicity of metals and metal oxides results from the indirect formation of ROS. Protonation of O_2 radicals can produce hydroxyl and peroxy radicals (OH, H_2O_2), which in turn can convert fatty acids to toxic lipid peroxides, destroying biological membranes.[43] Moreover, amorphous TiO_2 particles produced more ROS than anatase TiO_2 particles of the same size.[21,22] In addition, it was unambiguously shown that 100% anatase TiO_2 particles (40–50 nm) resulted in higher ROS activities than anatase–rutile mixtures of the same size.[21,44] In addition to anatase–rutile mixtures, rutile TiO_2 particles also lead to decreased ROS activity compared to both amorphous and anatase TiO_2. It appears then that ROS activity of anatase–rutile TiO_2 decreased as the fraction of rutile increased.

Based on the hypothesis that crystallinity will affect oxidant generation,[21] we investigated whether the cytotoxicity of TiO_2 nanoparticles depends on the crystal phase. The effect of the crystal phase on TiO_2 activity was evaluated by comparing nanotoxicity of TiO_2 dispersions with nanoparticles of similar sizes and different nanostructure, namely anatase (100%) and Evonik P25 (anatase–rutile mixture [75%:25%]). Since these nanoparticles create aggregates, increasing their final size in the dispersion, ultrasonication was used to eliminate aggregation in aqueous suspensions and reduce their size.[45–48] Three different mechanisms – rupture, erosion, and shattering of nanoparticle cluster breakup – were reported by Özcan-Taşkin et al.[49] Following ultrasonication, characterization of TiO_2 100% anatase and Evonik P25 nanoparticles was performed to explore properties of the materials used in this study. DLS was used to characterize the size of TiO_2 nanoparticles. Periodic DLS measurements of the samples showed that the particle aggregates remained quite stable, as their hydrodynamic radius did not increase for a period of more than a week.[50] The average size was about 111.3 nm for TiO_2 100% anatase and 138.5 nm for Evonik TiO_2 P25, thus the two dispersions were of the same order of magnitude. The zeta potential of both dispersions was also quite similar: −16.7±9 mV for TiO_2 100% anatase, and −11.7±8 mV for Evonik TiO_2 P25.

Our results demonstrated that TiO_2 100% anatase was more efficient in inducing apoptotic cell death in MDA-MB-468 cells than Evonik TiO_2 P25. Apparently then, the highly malignant MDA-MB-468 cancer cells are more susceptible to UVA-activated TiO_2 nanoparticle-induced cell death compared to MCF-7 cells. It is possible then that the higher cytotoxic activity of TiO_2 100% anatase is a consequence of its pure anatase nanostructure. Our results are in agreement with the findings of Sayes et al[9] who demonstrated that nano-TiO_2 particles in the anatase phase generated the most ROS and the greatest cytotoxic responses following in vitro exposure of human dermal fibroblasts or A549 human lung epithelial cells. They concluded that the nano-TiO_2 particles in the anatase crystal phase were more efficient as photocatalysts compared to the rutile particles, due to inherent differences in the crystal structure of the two phases.[9]

Caspases are involved in the implementation of apoptotic process, since activation of these proteins result in impaired

cell function.[28,51] PARP is one of the main cleavage targets of caspases. During apoptosis, PARP is cleaved into 89 kDa and 24 kDa fragments that are inactive, since the small fragment containing the DNA-binding domain of cleaved PARP may inhibit access by other repair enzymes.[52] The 89 kDa fragment is localized to the nucleoplasm during apoptosis, in order to modulate the activity of other proteins involved in apoptosis, such as p53.[31,53]

Analysis of caspase-mediated PARP cleavage revealed that in MDA-MB-468 cells treated with TiO_2 100% anatase or photoexcited TiO_2 100% anatase nanoparticles, PARP cleavage was remarkably increased, confirming that TiO_2 100% anatase nanoparticles induced apoptosis in MDA-MB-468 cells; under the same conditions, PARP cleavage was not detected in MCF-7 cells. Similarly, photoexcited Evonik TiO_2 P25 treatment resulted in PARP cleavage in MDA-MB-468 cells, although this effect was less intense compared to the effect of TiO_2 100% anatase.

Bcl-2 family proteins play a crucial role in cell survival, since members of this family exert their effects regulating mitochondrial permeability.[54,55] Several studies have pointed out the apoptotic effect of Evonik TiO_2 P25 on lymphocytes,[56] reported time-dependent PARP cleavage induced by TiO_2 nanoparticles,[57] and demonstrated increased expression of the proapoptotic protein Bax, which activated caspase-9 and caspase-3,[33,34] following treatment of HeLa (human cervical adenocarcinoma) cells with TiO_2.[58] Moreover, Meena et al suggested that nano-TiO_2-induced oxidative stress and apoptosis occurred in a time- and dose-dependent manner.[59] In addition, the activation of p53, Bax, caspase-3, and oxidative DNA damage was involved in the mechanistic pathways of nano-TiO_2-induced apoptosis in human embryonic kidney (HEK)-293 cells.[59] According to our data, photoexcited TiO_2 100% anatase and Evonik P25 nanoparticles increased the expression of proapoptotic Bax in MDA-MB-468 cells, thus establishing an apoptotic mechanism involving caspase-mediated PARP inactivation. In contrast, none of the dispersions of photoexcited TiO_2 nanoparticles affected Bax expression in MCF-7 cells.

The late stages of apoptosis are characterized by damage (fragmentation) of DNA. DNA destruction was reported in human embryonic kidney cells and lymphocytes treated with TiO_2 nanoparticles.[59–61] We demonstrated that DNA damage indeed occurred specifically in the highly invasive MDA-MB-468 cells treated with photoexcited Sigma-Aldrich TiO_2 100% anatase or Evonik TiO_2 P25.

Taken together, our results indicated that the mechanism of TiO_2 nanoparticles' cytotoxicity involves increased Bax expression and caspase-mediated PARP cleavage, thus resulting in DNA fragmentation and cell apoptosis. As we have previously shown, small TiO_2 nanoparticles (2–3 nm) induced apoptosis specifically in MDA-MB-468 cells.[8] Our data also demonstrated that the cytotoxicity of TiO_2 nanoparticles is cell type-dependent, since MCF-7 cells at concentrations up to 20 μM TiO_2 were less susceptible to TiO_2-induced damage, compared to MDA-MB-468. These differences may be attributed to the different protein composition of the cell membrane affecting the manner that membrane proteins interact with TiO_2 particles.[16,62,63]

The observed photocatalytic cell-killing effect of TiO_2 nanoparticles on human epithelial breast carcinoma MDA-MB-468 cells could possibly assist other means of cancer treatment. Since UVA irradiation is harmful for cells, chemical doping of TiO_2 nanoparticles with nonmetals (nitrogen, fluorine, sulfur, carbon), thus allowing activation using visible light or metals (silver), would eliminate the requirement for UVA irradiation. Then, doped TiO_2 nanoparticles could possibly be used as an anticancer regimen applied locally, followed by light irradiation focused on the tumor. Cancer cells can be selectively killed, as the light beam can be introduced via a fiber optic near a tumor region, where titanium oxide photocatalysts are also applied by simple injection.[6]

Conclusion

The potential antitumor effects of photoactivated TiO_2 dispersions, nanostructured TiO_2 100% anatase, and Evonik TiO_2 P25 in cultured MCF-7 and MDA-MB-468 breast cancer epithelial cells were examined. We documented that the cytotoxicity of TiO_2 nanoparticles of similar size but different crystal structure gradually decreased as their composition changed from pure anatase to anatase–rutile mixtures. We demonstrated that photoexcited TiO_2 in a pure anatase structure induced apoptosis specifically in MDA-MB-468 cells. Although the accurate molecular mechanism involved in the preferential death of highly malignant cancer cells awaits additional exploration, the obtained results indicate that the molecular mechanism of TiO_2 nanoparticle cytotoxicity involves increased proapoptotic Bax expression, caspase-mediated PARP cleavage, and DNA fragmentation, thus resulting in cell apoptosis.

Acknowledgments

This research was cofinanced by the European Union (European Social Fund [ESF]) and Greek national funds through the Operational Programme "Education and Lifelong Learning" of the National Strategic Reference Framework (NSRF) Heracleitus II research funding program. Investing in knowledge

society through the European Social Fund. This research was also financed by the General Secretariat of Research and Technology, Ministry of Education and Religious Affairs (Action: "KRHPIS", Title: "Identification of targets for diagnosis and treatment of diseases" DIAS OPS 448325).

Disclosure

The authors report no conflicts of interest in this work.

References

1. Harman TC, Taylor PJ, Walsh MP, LaForge BE. Quantum dot superlattice thermoelectric materials and devices. *Science*. 2002;297:2229–2232.
2. McDonald SA, Konstantatos G, Zhang SG, et al. Solution-processed PbS quantum dot infrared photodetectors and photovoltaics. *Nat Mater*. 2005;4:138–142.
3. Oberdörster G, Maynard A, Donaldson K, et al. Principles for characterizing the potential human health effects from exposure to nanomaterials: elements of a screening strategy. *Part Fibre Toxicol*. 2005;2:8.
4. Oberdörster G, Oberdörster E, Oberdörster J. Nanotoxicology: an emerging discipline evolving from studies of ultrafine particles. *Environ Health Perspect*. 2005;113:823–839.
5. Oberdörster G, Stone V, Donaldson K. Toxicology of nanoparticles: a historical perspective. *Nanotoxicology*. 2007;1:2–25.
6. Fujishima A, Hashimoto K, Watanabe T. *TiO_2 Photocatalysis: Fundamentals and Applications*. Tokyo: BKC; 1999.
7. Choi H, Stathatos E, Dionysiou DD. Sol-gel preparation of mesoporous photocatalytic TiO_2 films and TiO_2/Al_2O_3 composite membranes for environmental applications. *Appl Catal B*. 2006;63:60–67.
8. Lagopati N, Kitsiou PV, Kontos AI, et al. Photo-induced treatment of breast epithelial cancer cells using nanostructured titanium dioxide solution. *J Photochem Photobiol A Chem*. 2010;214:215–223.
9. Sayes CM, Wahi R, Kurian PA, et al. Correlating nanoscale titania structure with toxicity: a cytotoxicity and inflammatory response study with human dermal fibroblasts and human lung epithelial cells. *Toxicol Sci*. 2006;92:174–185.
10. Stefanou E, Evangelou A, Falaras P. Effects of UV-irradiated titania nanoparticles on cell proliferation, cancer metastasis and promotion. *Catal Today*. 2010;151:58–63.
11. Falaras P. Synergetic effect of carboxylic acid functional groups and fractal surface characteristics for efficient dye sensitization of titanium oxide. *Sol Energy Mater Sol Cells*. 1998;53:163–175.
12. Wang ML, Tuli R, Manner PA, Sharkey PF, Hall DJ, Tuan RS. Direct and indirect induction of apoptosis in human mesenchymal stem cells in response to titanium particles. *J Orthop Res*. 2003;21:697–707.
13. Pioletti DP, Takei H, Kwon SY, Wood D, Sung KL. The cytotoxic effect of titanium particles phagocytosed by osteoblasts. *J Biomed Mater Res*. 1999;46:399–407.
14. Huang NP, Xu MH, Yuan CW, Yu RR. The study of the photokilling effect and mechanism of ultrafine TiO_2 particles on U937 cells. *J Photochem Photobiol A Chem*. 1997;108:229–233.
15. Zhang AP, Sun YP. Photocatalytic killing effect of TiO_2 nanoparticles on LS-174-T human colon cancer cells. *World J Gastroenterol*. 2004;10:3191–3193.
16. Song M, Zhang R, Dai Y, et al. The in vitro inhibition of multidrug resistance by combined nanoparticulate titanium dioxide and UV irradiation. *Biomaterials*. 2006;27:4230–4238.
17. Hirakawa K, Mori M, Yoshida M, Oikawab S, Kawanishi S. Photo-irradiated titanium dioxide catalyzes site specific DNA damage via generation of hydrogen peroxide. *Free Radic Res*. 2004;38:439–447.
18. Linsebigler AL, Lu G, Yates JT Jr. Photocatalysis on TiO_2 surfaces: principles, mechanisms, and selected results. *Chem Rev*. 1995;95:735–758.
19. Warheit DB, Webb TR, Sayes CM, Colvin VL, Reed KL. Pulmonary instillation studies with nanoscale TiO_2 rods and dots in rats: toxicity is not dependent upon particle size and surface area. *J Toxicol Sci*. 2006;91:227–236.
20. Warheit DB, Webb TR, Reed KL, Frerichs S, Sayes CM. Pulmonary toxicity study in rats with three forms of ultrafine-TiO_2 particles: differential responses related to surface properties. *Toxicology*. 2007;230:90–104.
21. Jiang J, Oberdörster G, Elder A, Gelein R, Mercer P, Biswas P. Does nanoparticle activity depend upon size and crystal phase? *Nanotoxicology*. 2008;2:33–42.
22. Venkatachari P, Hopke PK, Grover BD, Eatough DJ. Measurement of particle-bound reactive oxygen species in Rubidoux aerosols. *J Atmos Chem*. 2005;50:49–58.
23. Donaldson K, Aitken R, Tran L, et al. Carbon nanotubes: a review of their properties in relation to pulmonary toxicology and workplace safety. *J Toxicol Sci*. 2006;92:5–22.
24. Hoshino A, Fujioka K, Oku T, et al. Physicochemical properties and cellular toxicity of nanocrystal quantum dots depend on their surface modification. *Nano Lett*. 2004;4:2163–2169.
25. Berne BJ, Pecora R. *Dynamic Light Scattering*. Mineola (NY): Courier Dover; 2000.
26. Mosmann T. Colorimetric assay for cellular growth and survival: application to proliferation and cytotoxicity assays. *J Immunol Methods*. 1983;65:55–63.
27. Plumb JA. Cell sensitivity assays: the MTT assay. *Methods Mol Med*. 2004;88:165–169.
28. Hui H, Dotta F, Di Mario U, Perfetti R. Role of caspases in the regulation of apoptotic pancreatic islet beta-cells death. *J Cell Physiol*. 2004;200:177–200.
29. Tewari M, Quan LT, O'Rourke LT, et al. Yama/CPP32β, a mammalian homolog of CED-3, is a CrmA-inhibitable protease that cleaves the death substrate poly(ADP-ribose) polymerase. *Cell*. 1995;81:801–809.
30. Satoh MS, Lindahl T. Role of poly(ADP-ribose) formation in DNA repair. *Nature*. 1992;356:356–358.
31. Alvarez-Gonzalez R, Spring H, Müller M, Bürkle A. Selective loss of poly(ADP-ribose) and the 85-kDa fragment of poly(ADP-ribose) polymerase in nucleoli during alkylation-induced apoptosis of HeLa cells. *J Biol Chem*. 1999;274:32122–32126.
32. Oliver FJ, de la Rubia G, Rolli V, Ruiz-Ruiz MC, de Murcia G, Murcia JM. Importance of poly(ADP-ribose) polymerase and its cleavage in apoptosis, Lesson from an uncleavable mutant. *J Biol Chem*. 1998;273:33533–33539.
33. Reed JC. Bcl-2 family proteins. *Oncogene*. 1998;17:3225–3236.
34. Gross A, McDonnell J, Korsmeyer S. BCL-2 family members and the mitochondria in apoptosis. *Genes Dev*. 1999;13:1899–1911.
35. Aaij C, Borst P. The gel electrophoresis of DNA. *Biochim Biophys Acta*. 1972;269:192–200.
36. Hayward GS, Smith MG. The chromosome of bacteriophage T5. I. Analysis of the single-stranded DNA fragments by agarose gel electrophoresis. *J Mol Biol*. 1972;63:383–395.
37. McDonell MW, Simon MN, Studier FW. Analysis of restriction fragments of T7 DNA and determination of molecular weights by electrophoresis in neutral and alkaline gels. *J Mol Biol*. 1977;110:119–146.
38. Sambrook J, Russell DW. *Molecular Cloning: A Laboratory Manual*. Cold Spring Harbor (NY): CSH Laboratory; 2001.
39. Satkauskas S, Bureau MF, Puc M, et al. Mechanisms of in vivo DNA electrotransfer: respective contributions of cell electropermeabilization and DNA electrophoresis. *Mol Therapy*. 2002;5:133–140.
40. Brody J, Kern S. History and principles of conductive media for standard DNA electrophoresis. *Anal Biochem*. 2004;333:1–13.
41. Reeves J, Davies S, Dodd N, Jha A. Hydroxyl radicals (*OH) are associated with titanium dioxide (TiO_2) nanoparticle-induced cytotoxicity and oxidative DNA damage in fish cells. *Mutat Res*. 2007;640:113–122.

42. Zhu R, Wang S, Chao J, Sun X, Yao S. Oxidative and binding effect of nanoTiO_2 on plasmid DNA and pepsin. Poster presented at: Second International Conference on Bioinformatics and Biomedical Engineering; May 16–18, 2008; Shanghai, China.
43. Zhang H, Jiang Y, He Z, Ma M. Cadmium accumulation and oxidative burst in garlic (*Allium sativum*). *J Plant Physiol*. 2005;162:977–984.
44. Hsiao IL, Huang YJ. Effects of various physicochemical characteristics on the toxicities of ZnO and TiO_2 nanoparticles toward human lung epithelial cells. *Sci Total Environ*. 2011;409(7):1219–1228.
45. Sato K, Li JG, Kamiya H, Ishigaki T. Ultrasonic dispersion of TiO_2 nanoparticles in aqueous suspension. *J Am Ceram Soc*. 2008;91:2481–2487.
46. Yousefi A, Allahverdi A, Hejazi P. Effective dispersion of nano-TiO_2 powder for enhancement of photocatalytic properties in cement mixes. *Constr Build Mater*. 2013;41:224–230.
47. Othman SH, Rashid SA, Mohd Ghazi TI, Abdullah N. Dispersion and stabilization of photocatalytic TiO_2 nanoparticles in aqueous suspension for coatings applications. *J Nanomater*. 2012;2012:718214.
48. Higashitani K, Yoshida K, Tanise N, Murata H. Dispersion of coagulated colloids by ultrasonication. *Colloids Surf A Physicochem Eng Asp*. 1993;81:167–175.
49. Özcan-Taşkin NG, Padron G, Voelkel A. Effect of particle type on the mechanisms of break up of nanoscale particle clusters. *Chem Eng Res Des*. 2009;87:468–473.
50. Schatzel K, Drewel M, Ahrens J. Suppression of multiple scattering in photon correlation spectroscopy. *J Phys Condens Matter*. 1990; 2 Suppl: SA393.
51. Nicholson DW, Ali A, Thornberry NA, et al. Identification and inhibition of the ICE/CED-3 protease necessary for mammalian apoptosis. *Nature*. 1995;376:17–18.
52. Smulson ME, Pang D, Jung M, et al. Irreversible binding of poly(ADP) ribose polymerase cleavage product to DNA ends revealed by atomic force microscopy: possible role in apoptosis. *Cancer Res*. 1998;58:3495–3498.
53. Malanga M, Pleschke JM, Kleczkowska HE, Althaus FR. Poly(ADP-ribose) binds to specific domains of p53 and alters its DNA binding functions. *J Biol Chem*. 1998;273:11839–11843.
54. Kelekar A, Thompson CB. Bcl-2-family proteins: the role of the BH3 domain in apoptosis. *Trends Cell Biol*. 1998;8:324–330.
55. Shimizu S, Narita M, Tsujimoto Y. Bcl-2 family proteins regulate the release of apoptogenic cytochrome C by the mitochondrial channel VDAC. *Nature*. 1999;399:483–487.
56. Kang SJ, Kim BM, Lee YJ, Hong SH, Chung HW. Titanium dioxide nanoparticles induce apoptosis through the JNK/p38-caspase-8-Bid pathway in phytohemagglutinin-stimulated human lymphocytes. *Biochem Biophys Res Commun*. 2009;386:682–687.
57. Zhao J, Bowman L, Zhang X, et al. Titanium dioxide (TiO_2) nanoparticles induce JB6 cell apoptosis through activation of the caspase-8/Bid and mitochondrial pathways. *J Toxicol Environ Health*. 2009;72:1141–1149.
58. Ramkumar KM, Manjula C, Gnanakumar G, et al. Oxidative stress-mediated cytotoxicity and apoptosis induction by TiO_2 nanofibers in HeLa cells. *Eur J Pharm Biopharm*. 2012;81:324–333.
59. Meena R, Rani M, Pal R, Rajamani P. Nano-TiO_2-induced apoptosis by oxidative stress-mediated DNA damage and activation of p53 in human embryonic kidney cells. *Appl Biochem Biotechnol*. 2012;167:791–808.
60. Ghosh M, Bandyopadhyay M, Mukherjee A. Genotoxicity of titanium dioxide (TiO_2) nanoparticles at two trophic levels: plant and human lymphocytes. *Chemosphere*. 2010;81:1253–1262.
61. Brunette DM, Tengvall P, Textor M, Thomsen P. *Titanium in Medicine: Material Science, Surface Science, Engineering, Biological Responses, and Medical Applications*. Heidelberg: Springer; 2001.
62. Croker A, Goodale D, Chu J, et al. High aldehyde dehydrogenase and expression of cancer stem cell markers selects for breast cancer cells with enhanced malignant and metastatic ability. *J Cell Mol Med*. 2009;13:2236–2252.
63. Thevenot P, Cho J, Wavhal D, Timmons R, Tang L. Surface chemistry influences cancer killing effect of TiO_2 nanoparticles. *Nanomedicine*. 2008;4:226–236.